Desalination and Water Treatment
www.deswater.com
doi: 10.1080/19443994.2014.990928

57 (2016) 3891–3903
February

Taylor & Francis
Taylor & Francis Group

Groundwater protection from lead contamination using granular dead anaerobic sludge biosorbent as permeable reactive barrier

Ayad A.H. Faisal*, Ziad T. Abd Ali

Department of Environmental Engineering, College of Engineering, University of Baghdad, Baghdad, Iraq, Tel. +964 7904208688; email: ayadabedalhamzafaisal@yahoo.com (A.A.H. Faisal), Tel. +964 7903433954; email: z.teach2000@yahoo.com (Z.T. Abd Ali)

Received 21 March 2014; Accepted 14 November 2014

ABSTRACT

This study investigated the performance of granular dead anaerobic sludge (GDAS) biosorbent as permeable reactive barrier (PRB) in removing lead from contaminated shallow groundwater. Batch tests were performed to characterize the equilibrium sorption properties of the GDAS and sandy soil in lead-containing aqueous solutions. Fourier transform infrared analysis proved that the carboxylic, alcohol, and alkyl halides groups were responsible for the biosorption of lead onto GDAS. A two-dimensional numerical model, solved by COMSOL Multiphysics 3.5a software, which is based on finite element method, was developed to simulate the equilibrium transport of lead within groundwater. This model considered the pollutant sorption onto the GDAS and sandy soil using Langmuir equation. Numerical and experimental results proved that the PRB plays a potential role in the restriction of the contaminant plume migration. Furthermore, the barrier started to saturate with contaminant as a function of the travel time, and thicker barrier was more efficient than thinner one. However, a good agreement between the predicted and experimental results was recognized with root mean squared error not exceeding 0.055.

Keywords: Granular dead anaerobic sludge; Lead; Permeable reactive barrier; Transport; Groundwater

1. Introduction

The presence of toxic heavy metals in groundwater brings about significant changes in the properties of water resources and must be avoided to preserve the environmental quality. Toxic heavy metals, such as mercury, chromium, and lead, can be related to many anthropogenic sources, and their compounds are extremely toxic [1]. The protection of groundwater and surface water is important, which needs to be resolved as fast as possible. Groundwater can be polluted mainly with pollutants from dumping sites, municipal landfills, petrol stations, airports, agriculture, and chemical plants. Contaminants from these sources can flow downward in the unsaturated zone, reach the groundwater, flow horizontally in the form of diluted solution, and pollute surface water such as rivers, lakes, etc. There are more than 30 types of technologies for treating groundwater and contaminated soil. Permeable reactive barrier (PRB) is an interesting passive method where contaminants are removed from an aquifer by the flow through a reactive barrier filled with a reactive material [2]. The main advantages of this technology are treatment of contaminants

*Corresponding author.

in the subsurface, complete plume capture, lower operation and maintenance costs, and lower long-term performance monitoring costs [3].

Presently, the global population overgrowth coupled with accelerating technological advances and concomitant environmental pollution/climate change have led to a significant reduction in water resource availability and appreciable deterioration of water quality. Iraq is currently facing severe water shortages across most parts of the country, with over 7.6 million Iraqis lacking access to safe drinking water and the agriculture sector suffering from years of water scarcity [4]. Accordingly, PRB technology could have a significant positive impact on the quality of groundwater resources, making it a reliable complementary option to surface water.

Sewage sludge is recognized as a valuable resource that can be recycled as fertilizer and soil improvement material for land, because it consists largely of organic substances and contains nitrogen and phosphorus, which are the main nutrimental elements of plants. Activated sludge is a well-known biosorbent used for the purification of some industrial effluents and domestic wastes. A part of the micro-organisms, over grown in such wastewater systems, can be separated and utilized for the removal of organic and inorganic pollutants as an abundant and cheaper biosorbent. The activated sludge from wastewater systems mainly consists of bacteria, protozoa, fungi, yeasts, and other micro-organisms, and is therefore considered as a heterogeneous biosorbent material. The protozoa are unicellular, motile, and relatively large eukaryotic cells that lack cell walls. They can adsorb components through their outer membranes that contain proteins and lipids [5]. Aerobic dried activated sludge has been used by many researchers to remove heavy metals and organic pollutants from industrial wastewater. In the present study, granular dead anaerobic sludge (GDAS) or dead biomass from drying beds, which is richer with different micro-organisms than aerobic activated sludge [6], was used as a biosorbent to remove lead from synthetic contaminated groundwater.

Considerable theoretical and experimental studies on PRBs using different types of reactive medium such as activated carbon, zeolite, and zero-valent iron (ZVI) for the removal of heavy metals from groundwater have been performed. For example, a set of batch and column tests were conducted to determine the design factors for clinoptilolite (one of the natural zeolites) PRBs for the treatment of groundwater contaminated with ammonium and heavy metals [7]. It has been reported that the removal of heavy metals from contaminated groundwater is possible on activated sludge using biosorption process, depending on the complex substances formed by the heavy metals and functional groups such as carboxyl, hydroxyl, and phenolic groups of the extracellular polymeric substances [8]. In a previous study, a continuous column experiment was conducted under dynamic flow conditions to study the efficiency of low-cost PRBs to remove several inorganic contaminants from acidic solutions. A 50:50 w/w waste iron/sand mixture was used as the candidate reactive medium to activate precipitation and promote sorption and reduction–oxidation mechanisms [9]. Furthermore, the treatment of the groundwater contaminated with metals by dumping sites located in the provinces of southern Poland was investigated. The simulated groundwater circulated through the column filled with ZVI in the laboratory tests. Chromium, copper, nickel, cobalt, lead, cadmium, and zinc, occurring in the water as cations and anions, were removed in the iron bed [10]. In another study, the performance of zeolite PRB in removing cadmium from a contaminated shallow aquifer was examined. Batch tests were performed to characterize the equilibrium sorption properties of the zeolite in cadmium-containing aqueous solutions. A one-dimensional numerical finite difference model was developed to describe pollutant transport within groundwater by considering pollutant sorption on the PRB [11]. Similarly, many other studies [12–17] had

Table 1
Physical and chemical characteristics of GDAS

Physical properties	Value	Chemical properties	Value
Actual density (kg/m^3)	1,741.6	pH	7.5
Apparent density (kg/m^3)	609.9	Ash content (%)	12
Surface area (m^2/g)	94.53	Cation exchange capacity (CEC, meq/100 g)	51.153
Bed porosity	0.45	Initial Pb^{2+} concentration (mg/kg)	≤30
Average particle diameter (mm)	0.775	Organic volatile solid (V·S, 10^6 mg/l)	0.135
Pore volume (cm^3/g)	0.544	Non-volatile solid (N·V.S, 10^6 mg/l)	0.018

been conducted to investigate the performance and efficacy of this technology under different conditions.

The regular biological activities of municipal wastewater treatment plants produce large quantities of byproduct biomass wastes. Thus, reuse of this waste as a reactive medium in PRBs is attractive in terms of sustainable development and reduced disposal costs. Accordingly, the aims of the present study were to: (1) investigate the potential application of GDAS biosorbent as an inexpensive material in PRBs for the removal of lead from contaminated groundwater; (2) determine the predominant functional groups that are responsible for lead removal in the GDAS biosorbent using Fourier transform infrared spectroscopy (FTIR) analysis; and (3) characterize the two-dimensional equilibrium transport of lead theoretically using COMSOL Multiphysics 3.5a (2008) software and experimentally using bench-scale model.

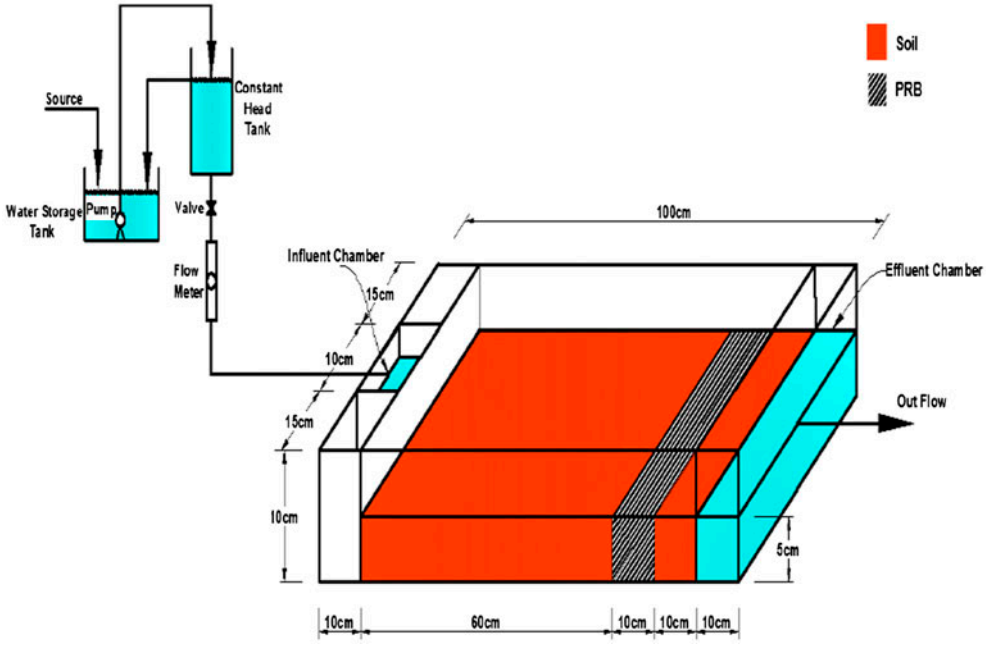

Fig. 1. Schematic diagram of the bench-scale model aquifer.

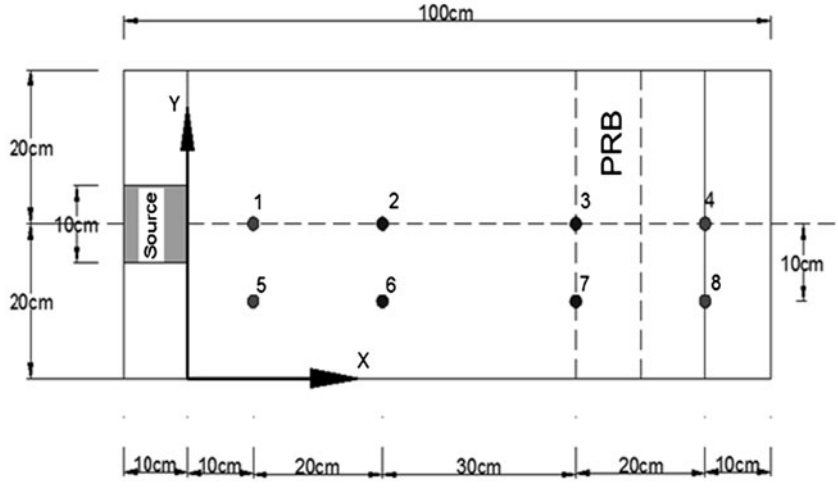

Fig. 2. Schematic diagram of the sampling plate and sampling ports.

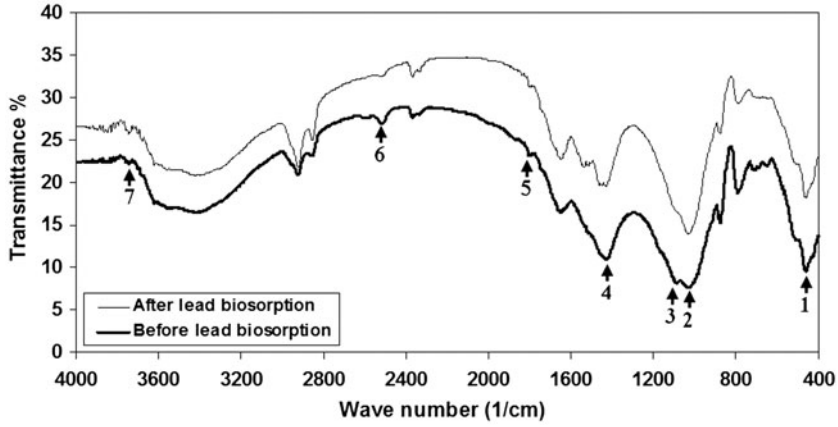

Fig. 3. FTIR analysis of GDAS before and after biosorption of lead.

Table 2
Functional groups responsible for lead biosorption onto GDAS

FTIR peak	Wave no. (cm^{-1})	Type of bond	Functional group
1	514.33	$–C–Br^-$	Alkyl halides
2	1,028.11	$–C–O–C^-$, OH^-	Alcohol, carboxylic acid
3	1,086.01	$–C–O–C^-$	Alcohol
4	1,421.03	$–OH^-$	Carboxylic acid
5	1,800.99	$–C=O^-$	Carboxylic acid
6	2,519.21	$–OH^-$	Carboxylic acid
7	3,740.11	$–OH^-$	Carboxylic acid

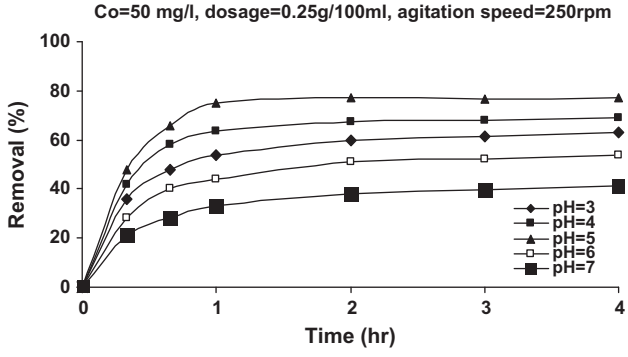

Fig. 4. Lead removal efficiency of lead on GDAS as a function of contact time and initial pH.

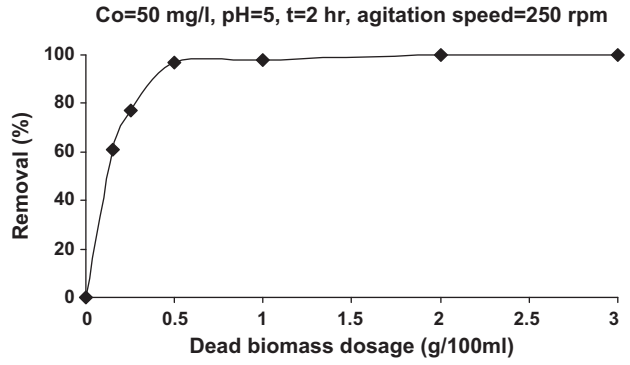

Fig. 5. Effect of GDAS dosage on the lead removal efficiencies.

2. Materials and methods

2.1. Medium and contaminant

The GDAS was dried at atmospheric temperature for 5 d and sieved using 1/0.6 mm diameter mesh. The sieved portion was washed five times with distilled water and dried at 70°C for 6 h prior to use [18]. Table 1 shows the physical and chemical characteristics of GDAS used in the present study.

The sandy soil, with porosity of 0.41, was used as aquifer in the experiments conducted. This soil had a particle size distribution ranging from 63 μm to 0.71 mm with an effective grain size (d_{10}) of 110 μm, a median grain size (d_{50}) of 180 μm, and a uniformity coefficient ($Cu = d_{60}/d_{10}$) of 1.73. The hydraulic conductivity and bulk density were 4.22×10^{-3} cm/s and 1.563 g/cm^3, respectively.

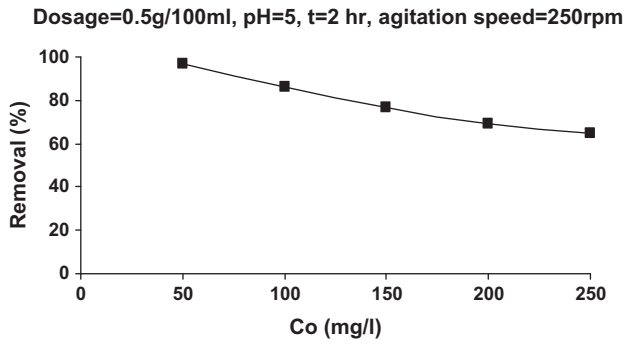

Fig. 6. Effect of initial concentration on the lead removal efficiency on GDAS.

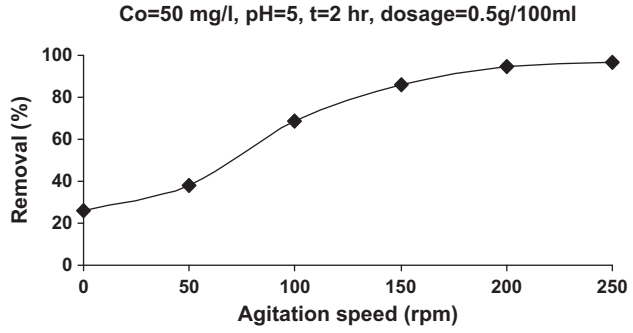

Fig. 7. Effect of agitation speed on the percentage removal of lead.

Table 3
Parameters of isotherm models for the biosorption of lead onto GDAS and soil

Isotherm model	Parameter	GDAS	Soil
Langmuir	b (l/mg)	0.0349	0.0133
	q_m (mg/g)	111.6	30.8
	R^2	0.9914	0.9893
Freundlich	K_F (mg/mg)(l/mg)$^{1/n}$	0.0079	0.0016
	n	3.0650	2.5893
	R^2	0.9893	0.8623
Elovich	q_m (mg/g)	9	–
	K_E (l/mg)	1.4670	
	R^2	0.9555	
Temkin	ΔQ (kJ/mol)	14.6770	–
	K_o (l/mg)	1.0009	
	R^2	0.9658	
Kiselev	k_1 (l/mg)	0.2785	–
	k_n	−0.8790	
	R^2	0.9123	
Hill–de Boer	k_1 (l/mg)	0.0136	–
	k_2 (kJ/mol)	24.7274	
	R^2	0.9345	

Lead was selected as a representative of heavy metal contaminants. To simulate the water's lead contamination, a solution of $Pb(NO_3)_2$ (manufactured by BDH, England) was prepared and added to the specimen to obtain representative concentration.

2.2. Batch experiments

Batch experiments were conducted to determine the best conditions of contact time, initial pH of the solution, initial concentration of the metal, dosage, and agitation speed. A series of 250 ml flasks was employed and each flask was filled with 100 ml of lead solution with an initial concentration of 50 mg/l. Subsequently, about 0.25 g of the adsorbent was added into these flasks and stirred in high-speed orbital shaker at 250 rpm for 4 h. A fixed volume (20 ml) of the solution was withdrawn from each flask and filtered to separate the adsorbent, and a fixed volume (10 ml) of the clear solution was pipetted out to determine the concentration of lead remaining in the solution. The measurements were conducted using atomic absorption spectrophotometer (AAS) (Shimadzu, Japan) and the adsorbed concentration of lead on the reactive material was determined by a mass balance.

Kinetic studies were performed at pH (3, 4, 5, 6, and 7), initial lead concentration (50, 100, 150, 200, and 250 mg/l), adsorbent dosage (0.15, 0.25, 0.5, 1, 2, and 3 g), and agitation speed (0, 50, 100, 150, 200, and 250 rpm). From the best experimental results, the amount of lead retained in the GDAS phase (q_e) was calculated as follows [19]:

$$q_e = (C_0 - C_e)\frac{V}{m} \quad (1)$$

where C_0 and C_e are the initial and equilibrium concentrations of lead in the solution (mg/l), V is the volume of the solution (l), and m is the mass of GDAS (g).

2.3. Description of sorption data

Six isotherm models were used for the description of sorption data as follows [20]:

- *Langmuir model*: This model assumes uniform energies of adsorption onto the surface and no transmigration of the adsorbate in the plane of the surface. It can be written as:

$$q_e = \frac{q_m\, b\, C_e}{1 + b\, C_e} \quad (2)$$

Table 4
Model geometry and boundary value problem for simulated two-dimensional problem adopted in the present study

Model geometry		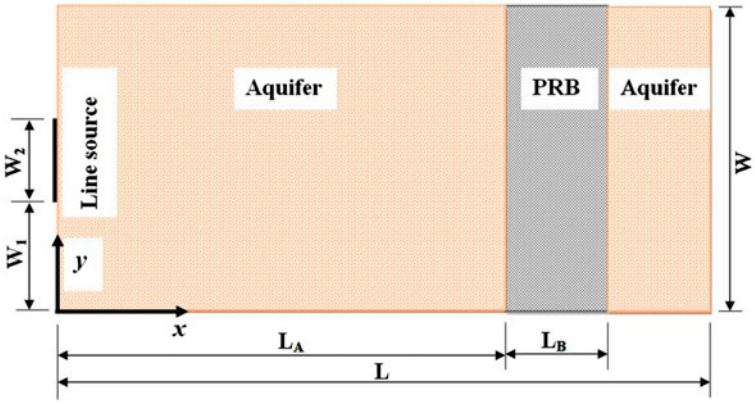
Equations	Aquifer (A)	$D_{Ax}\frac{\partial^2 C_A}{\partial x^2} + D_{Ay}\frac{\partial^2 C_A}{\partial y^2} - V_{Ax}\frac{\partial C_A}{\partial x} = R_A\frac{\partial C_A}{\partial t}$
	PRB (B)	$D_{Bx}\frac{\partial^2 C_B}{\partial x^2} + D_{By}\frac{\partial^2 C_B}{\partial y^2} - V_{Bx}\frac{\partial C_B}{\partial x} = R_B\frac{\partial C_B}{\partial t}$
Conditions	Aquifer (A)	I·C. (Initial condition) $C_A(x, y, 0) = 0$ Exterior B·C. (Boundary condition) $C_A(0, y, t) = 0$ except $C_A(0, y, t) = 50$ mg/l @ $W_1 \le y \le W_1 + W_2$ $\frac{\partial C_A}{\partial x} = 0$ @ (L, y, t) $\frac{\partial C_A}{\partial y}(x, 0, t) = 0$ and $\frac{\partial C_A}{\partial y}(x, W, t) = 0$ for $0 \le x \le L_A$, $L_A + L_B \le x \le L$ $\frac{\partial C_B}{\partial y}(x, 0, t) = 0$ and $\frac{\partial C_B}{\partial y}(x, W, t) = 0$ for $L_A \le x \le L_A + L_B$
	PRB (B)	I·C. $C_B(x, y, 0) = 0$ Interior B·C. $C_A(L_A, y, t) = C_B(L_A, y, t)$ $C_A(L_A + L_B, y, t) = C_B(L_A + L_B, y, t)$ $-D_{Bx}n_B\frac{\partial C_B}{\partial x} - D_{By}n_B\frac{\partial C_B}{\partial y} + V_{Bx}n_BC_B = -D_{Ax}n_A\frac{\partial C_A}{\partial x} - D_{Ay}n_A\frac{\partial C_A}{\partial y} + V_{Ax}n_AC_A$ @ (L_A, y, t) $-D_{Bx}n_B\frac{\partial C_B}{\partial x} - D_{By}n_B\frac{\partial C_B}{\partial y} + V_{Bx}n_BC_B = -D_{Ax}n_A\frac{\partial C_A}{\partial x} - D_{Ay}n_A\frac{\partial C_A}{\partial y}V_{Ax}n_A$ @ $(L_A + L_B, y, t)$

Note: C_A and C_B are the lead concentrations in the aquifer and PRB, respectively.

where q_m is the maximum adsorption capacity (mg/g) and b is the constant related to the free energy of adsorption (l/mg).

- *Freundlich model*: This model is quantified by:

$$q_e = K_F\, C_e^{1/n} \tag{3}$$

where K_F is the Freundlich sorption coefficient and n is an empirical coefficient indicative of the intensity of the adsorption.

- *Elovich model*: This model is based on a kinetic principle assuming that the adsorption sites increase exponentially with adsorption, which implies a multi-layer adsorption. It can be expressed as:

$$\frac{q_e}{q_m} = K_E\, C_e \exp\left(-\frac{q_e}{q_m}\right) \tag{4}$$

where K_E is the Elovich equilibrium constant (l/mg) and q_m is the Elovich maximum adsorption capacity (mg/g).

- Temkin model: This model assumes that the heat of adsorption of all the molecules in the layer decreases linearly with coverage owing to the adsorbent–adsorbate interactions, and that the

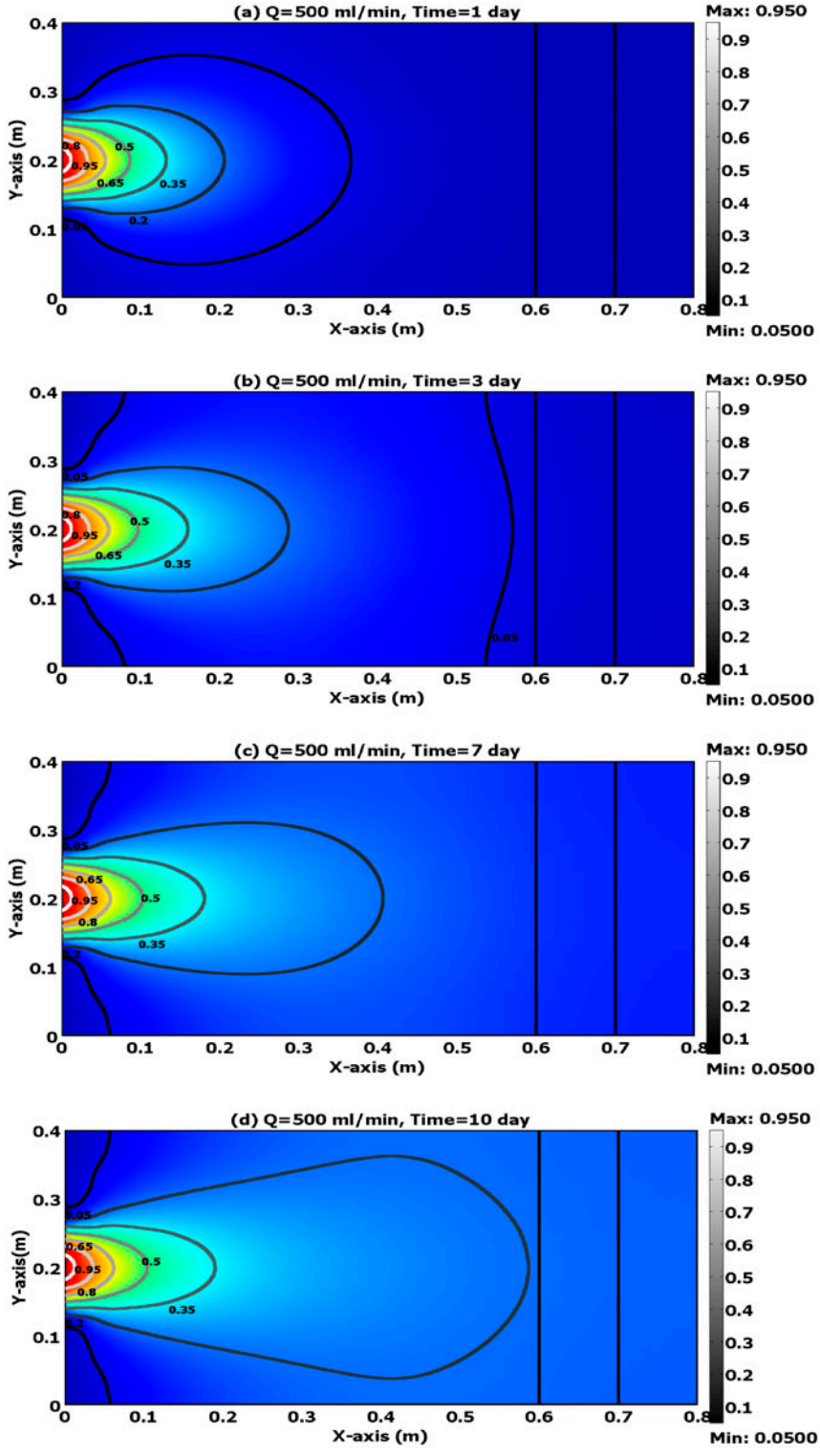

Fig. 8. Distribution of lead concentration after (a) 1, (b) 3, (c) 7, and (d) 10 d for a flow rate of 500 ml/min using GDAS as the PRB.

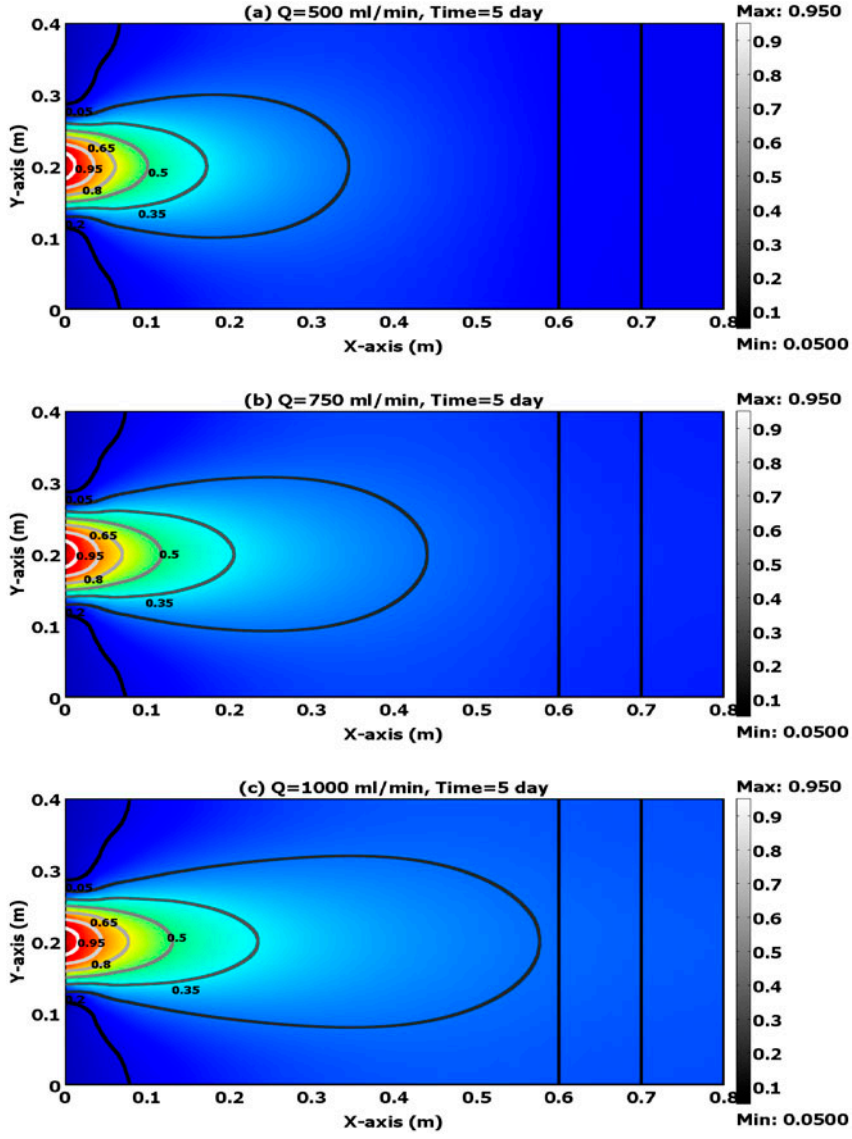

Fig. 9. Distribution of lead concentration after 5 d for a flow rate of (a) 500, (b) 750, and (c) 1,000 ml/min using GDAS as the PRB.

adsorption is characterized by a uniform distribution of the binding energies, up to some maximum binding energy. It can be expressed as:

$$\theta = \frac{RT}{\Delta Q} \ln K_o C_e \tag{5}$$

where θ ($=q_e/q_m$) is the fractional coverage, R is the universal gas constant (kJ/mol/K), T is the temperature (K), ΔQ is the variation of adsorption energy (kJ/mol), and K_o is the Temkin equilibrium constant (l/mg).

- *Kiselev model*: This model is known as the adsorption isotherm in localized monomolecular layer and can be expressed as:

$$k_1 C_e = \frac{\theta}{(1-\theta)(1+k_n\theta)} \tag{6}$$

where k_1 is the Kiselev equilibrium constant (l/mg), θ ($=q_e/q_m$) is the fractional coverage, and k_n is the

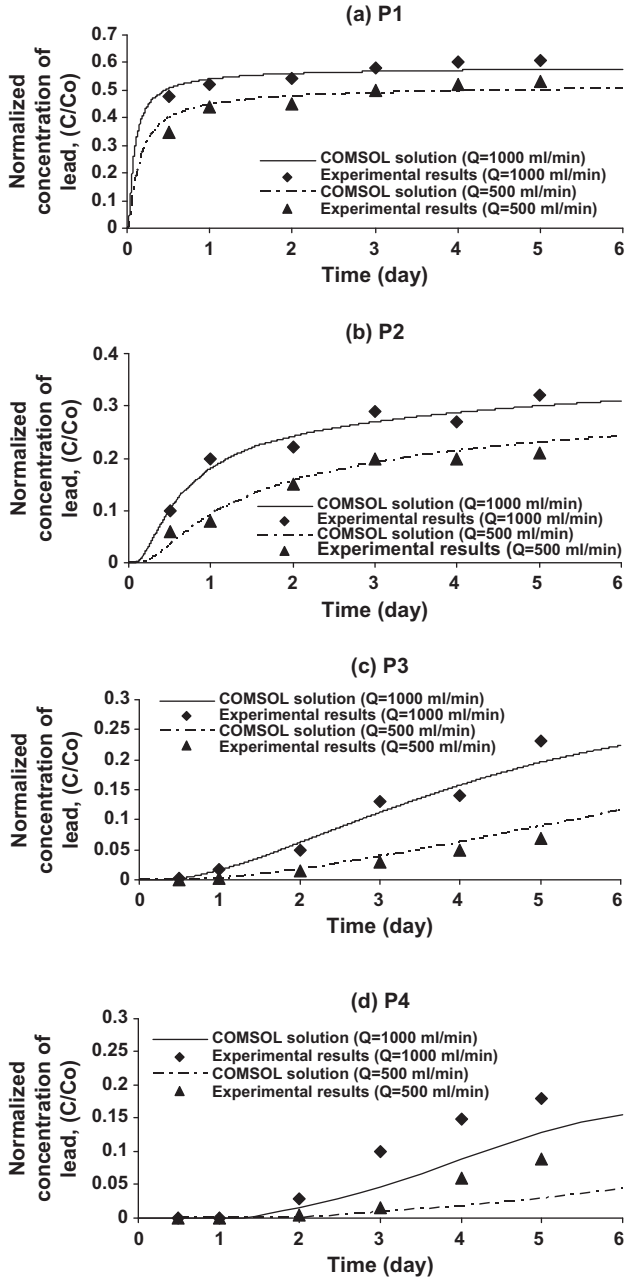

Fig. 10. Breakthrough curves as a result of lead transport at ports (a) P1, (b) P2, (c) P3, and (d) P4 for different flow rates using GDAS as the PRB.

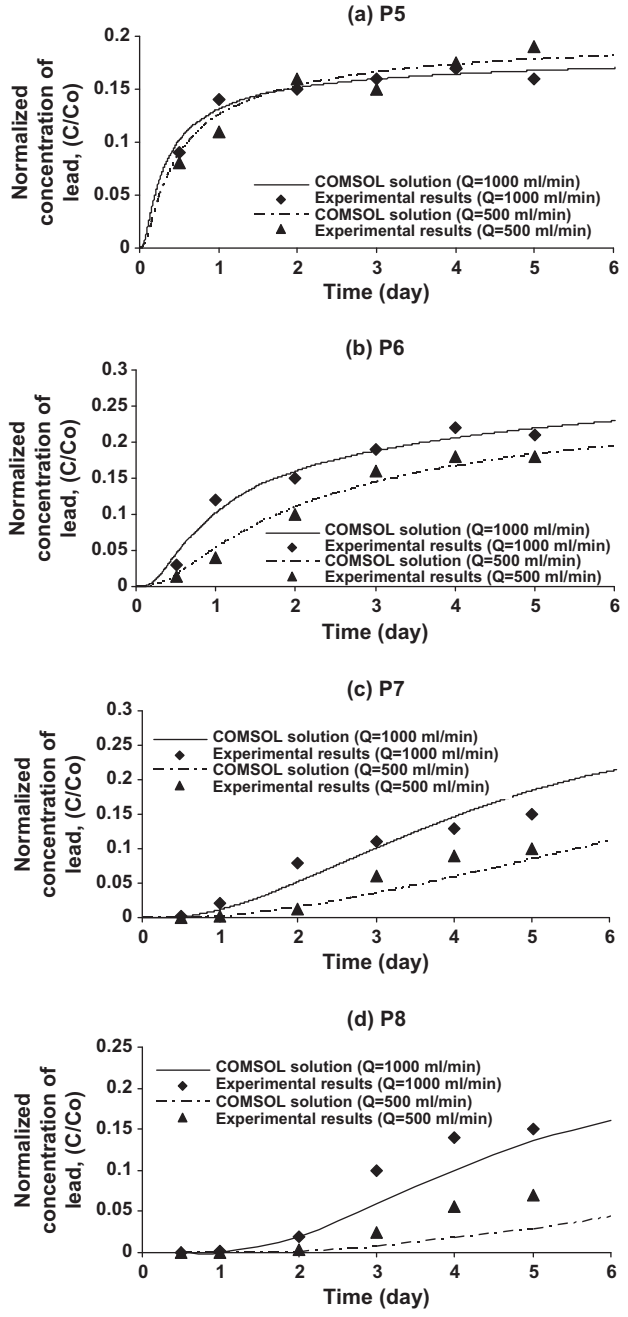

Fig. 11. Breakthrough curves as a result of lead transport at ports (a) P5, (b) P6, (c) P7, and (d) P8 for different flow rates using GDAS as the PRB.

constant of complex formation between the adsorbed molecules.

- Hill–de Boer model: This model describes the case where there are mobile adsorption and lateral interaction among the adsorbed molecules and is given by:

$$k_1 C_e = \frac{\theta}{1-\theta}\exp\left(\frac{\theta}{1-\theta} - \frac{k_2\theta}{RT}\right) \quad (7)$$

where k_1 is the Hill–de Boer constant (l/mg) and k_2 is the energetic constant of the interaction between the adsorbed molecules (kJ/mol).

2.4. Two-dimensional continuous experiments

Fig. 1 shows the schematic diagram of the bench-scale model aquifer used in the present study. The simulated lead transport was performed in a two-dimensional tank. The bench-scale model aquifer was placed within a 6 mm thick rectangular Perspex glass tank (80 × 40 × 10 cm). All the sides of the tank were transparent to allow visual observations. Two vertical perforated plates covered with filtration screen were used as partitions. These partitions provided the lateral boundaries of the sand-filled middle compartment with a dimension of 80 × 40 × 10 cm. The purpose of the two outer compartments, i.e. influent and effluent chambers, was to control the position of the watertable within the model aquifer placed in the middle compartment and to regulate the wetting of this aquifer mass. Each outer compartment had a dimension of 10 × 40 × 10 cm. The flow through the model aquifer was accomplished by a storage tank, two constant head tanks, and a flow-meter. Two flow rates (500 and 1,000 ml/min) were selected with corresponding seepage velocities of 87.8 and 175.6 m/d, respectively.

The sampling plate (Fig. 2) was placed on top of the Perspex glass tank to support the sampling ports. This plate contained 4 columns and 2 rows of sampling ports designated from P1 to P8. The aqueous samples from the model aquifer were collected using stainless syringes at specified periods. The lead-contaminated solution with a concentration of 50 mg/l was introduced through the model aquifer from the cubic source, which was located at the side of the aquifer. This source (10 × 10 × 10 cm) simulated continuous release of contaminants.

At the beginning of each test, the middle compartment was packed with 5 cm depth model aquifer. The model aquifer consisted of three parts. The first part was 60 cm of sandy soil measured from the left side of the tank. The second part was a 10 cm barrier of reactive material placed beside the packed soil. The third part was 10 cm of sandy soil placed beside this barrier. The aquifer was filled with water and left overnight to settle and saturate this soil. Then, the packed aquifer was flushed at maximum velocity until the effluent water was free of suspended fine material.

The lead concentrations within the aquifer model in the effluent from sampling ports were monitored for a period of 5 d. The water samples (3–5 ml) were regularly collected (after 0.5, 1, 2, 3, 4, and 5 d) from each port, and immediately added to glass vials and analyzed by AAS. At the end of each experiment, the soil was removed from the tank. The tank was soaked in a dilute NaOH solution and rinsed first with tap water, and finally with distilled water to avoid cross-contamination between the experiments.

2.5. Fourier-transform infrared analysis

This analysis has been considered as a direct method for investigating the sorption mechanisms by identifying the functional groups responsible for the binding of lead onto GDAS [21]. The characteristic bands of the GDAS before and after lead uptake at a pH of 5 were used to assess the changes in the functional groups of this material. A 250 ml flask was filled with 100 ml of the contaminant solution containing 50 mg/l lead and 0.5 g of GDAS. The flask was agitated for an equilibrium time at 250 rpm. The infrared spectra of the GDAS samples before and after lead biosorption were examined using Shimadzu FTIR, 800 series spectrophotometer, Japan.

3. Results and discussion

3.1. FTIR analysis

The infrared spectra of the GDAS samples, measured with the range of 400–4,000 cm^{-1}, before and after biosorption of lead were examined (Fig. 3). The functional groups identified in the GDAS and their contributions in the biosorption process of lead are summarized in Table 2. The shifts in the infrared frequencies indicated that the carboxylic, alcohol, and alkyl halides groups were responsible for the biosorption of lead onto GDAS [22].

3.2. Influence of batch operating parameters

Fig. 4 shows the effect of contact time and initial pH of the solution on lead sorption using 0.25 g of GDAS added to 100 ml of metal solution, determined by batch experiments conducted at 25˚C. The adsorption rate was initially very fast and increased with increasing contact time, until it reached the equilibrium time (= 2 h). This may be owing to the presence of a large number of adsorbent sites available for the adsorption of the metal ions. Furthermore, the increase in the metal removal with the increasing pH can be explained by the decrease in the competition between the proton and metal species for the surface sites, and the decrease in positive surface charge, resulting in a lower columbic repulsion of the sorbing metal [23]. Thus, it is clear that the maximum removal efficiency of lead was achieved at an initial pH of 5.

Fig. 5 shows that the lead removal efficiency on GDAS improved with increasing adsorbent dosage

from 0.15 to 0.5 g for a fixed initial metal concentration. This result was expected owing to the fact that the availability of sorption sites increases with the increasing dose of adsorbents in the solution.

Fig. 6 indicates that the removal efficiency decreased from 97 to 65% with the increasing initial lead concentration from 50 to 250 mg/l. This finding signifies that energetically less favorable sites become involved with increasing lead concentrations in the aqueous solution [24].

Fig. 7 shows the gradual increase in contaminants uptake when the agitation speed was increased from 0 to 250 rpm, at which about 97% of lead was removed. This can be attributed to the improved diffusion of ions toward the surface of the reactive medium and, consequently, suitable contact between the ions in the solution and binding sites.

3.3. Sorption isotherms

The sorption data for lead on GDAS were fitted with a linearized form of Langmuir, Freundlich, Temkin, Elovich, Kiselev, and Hill–de Boer models. In addition, the sorption data of sandy soil were fitted only with Langmuir and Freundlich models. Table 3 presents the fitted parameters and coefficient of determination (R^2) for each model. It is clear that the Langmuir isotherm model provided the best correlation, when compared with the other models. Accordingly, the Langmuir model was used to describe the sorption of lead onto GDAS and sandy soil in the partial differential equation (PDE) governed by the transport of a solute in continuous mode.

3.4. Longitudinal dispersion coefficient

The results of the experimental runs concerning the measurement of longitudinal dispersion coefficient (D_L) at different velocities (V) for soil and GDAS took a linear relationship as follows:

$$D_L = 22.900\ V + 0.871 \qquad R^2 = 0.9172 \qquad \text{[Soil]} \tag{8}$$

$$D_L = 53.944\ V + 0.297 \qquad R^2 = 0.9792 \qquad \text{[GDAS]} \tag{9}$$

This indicated that the longitudinal dispersivity (α_L) was equal to 22.9 and 53.944 cm for soil and GDAS, respectively.

3.5. Two-dimensional model development

The contaminant migration in a porous medium is due to the advection–dispersion processes; therefore, considering a two-dimensional system (unidirectional fluid flow and two-dimensional transient solute transport), the dissolved lead mass balance equation can be written as follows:

$$D_x \frac{\partial^2 C}{\partial x^2} + D_y \frac{\partial^2 C}{\partial y^2} - V_x \frac{\partial C}{\partial x} = \frac{\partial C}{\partial t} + \frac{\rho_b}{n} \frac{\partial q}{\partial t} \tag{10}$$

where C is the lead concentration in water, q is the lead concentration on solid, and ρ_b is the dry adsorbing material bulk density. Under the isotherm conditions, the second term (q) on the right-hand side of this equation can be replaced with Langmuir model (Eq. (2)). Table 4 summarizes the model geometry and boundary value problem (i.e. governing equations, initial conditions, and boundary conditions) for the simulated two-dimensional problem adopted in the present study.

Fig. 8 describes the predicted surface and contour plot of normalized concentrations of lead across the laboratory two-dimensional sandy soil packed tank in the presence of PRB after 1, 3, 7, and 10 d for a flow rate of 500 ml/min. It is clear that the propagation of the contaminated plume is restricted by the GDAS

Table 5
Comparison between predicted removal efficiencies of the lead for two values of PRB thickness

Travel time (d)	Removal efficiency of lead (%)[a]	
	Thickness of barrier = 10 cm	Thickness of barrier = 15 cm
1	75	90
2	53	72
3	35	60
4	25	50
5	20	40

[a]The thickness of the barrier measured from X = 60 cm.

barrier and the functionality of the barrier decreases with the time because of the decreasing retardation factor.

Fig. 9 shows the effect of the applied flow rate, i.e. velocity of flow, on the extent and concentration magnitudes of the lead plume. It can be clearly noted that the extent of contaminant plume in the longitudinal (X) direction is greater than that in the transverse (Y) direction, which is consistent with the assumption of unidirectional velocity adopted in the present study. Moreover, the highest concentrations were observed in the sand bed, which is the up-gradient of PRB. Thus, it is evident that the functionality of the barrier will decrease with the increasing velocity of flow because of the greater penetration of the contaminant plume.

Figs. 10 and 11 present the comparison between the predicted and experimental results at the nodes corresponding to the monitoring ports (P1–P8) during the migration of the lead plume at different periods of time, and flow rates of 500 and 1,000 ml/min. The lead concentrations in the ports (P1, P2, P3, and P4) located along the centerline of the source area ($Y = 20$ cm) were higher than those in the ports (P5, P6, P7, and P8) deviated from the centerline by 10 cm (i.e. $Y = 10$ cm). In addition, it can be noted from Table 5 that the potential functionality of the GDAS as a function of its thickness in the retardation of lead migration represented by COMSOL predicted removal efficiency in the location just before ($X = 60$ cm and $Y = 20$ cm) and beyond the barrier ($X = 70$ cm and $Y = 20$ cm), and it appeared that the increased thickness of PRB could increase the removal efficiency. A good agreement between the predicted and experimental results was observed with root mean squared error (RMSE) [25] not exceeding 0.055.

4. Conclusions

From the batch experiments, the best values of the parameters that affected lead biosorption/sorption process onto GDAS and sandy soil were noted to be contact time of 2 h, initial pH of the solution of 5, initial lead concentration of 50 mg/l, sorbent dosage of 0.5 g/100 ml, and agitation speed of 250 rpm. The sorption data were reasonably well correlated by the Langmuir sorption isotherm with coefficient of determination (R^2) greater than 0.989. Furthermore, FTIR analysis proved that the carboxylic, alcohol, and alkyl halides groups were responsible for the biosorption of lead onto GDAS.

The results of two-dimensional numerical model solved by COMSOL Multiphysics 3.5a under equilibrium condition proved that the GDAS barrier was efficient in the restriction of contaminant plume. The results proved that the functionality of the barrier decreased with the increasing travel time and velocity of flow. However, this functionality increased with increasing barrier thickness. A good agreement between the predicted and experimental results was recognized with RMSE not exceeding 0.055.

References

[1] F. Di Natale, M. Di Natale, R. Greco, A. Lancia, C. Laudante, D. Musmarra, Groundwater protection from cadmium contamination by permeable reactive barriers, J. Hazard. Mater. 160 (2008) 428–434.
[2] J. Mieles, H. Zhan, Analytical solutions of one-dimensional multispecies reactive transport in a permeable reactive barrier-aquifer system, J. Contam. Hydrol. 134–135 (2012) 54–68.
[3] W.W. Powell, W. Kenneth, J. Koput, I. Bowie, S.D. Laurel, The spatial clustering of science and capital: Accounting for biotech firm—Venture capital relationships, Reg. Stud. 36 (2002) 299–313.
[4] UNESCO, Launches Initiative to Identify Groundwater and Alleviate Water Shortages in Iraq (2010). Available from: <www.unesco.org/.../iraq.../unesco_launches_initiative_to_identify_groun>.
[5] Z. Aksu, J. Yener, A comparative adsorption/biosorption study of mono-chlorinated phenols onto various sorbents, Waste Manage. 21 (2001) 695–702.
[6] Metcalf & Eddy, Wastewater Treatment, Disposal and Reuse, McGraw-Hill, New York, NY, 1991.
[7] J.B. Park, S.H. Lee, J.W. Lee, C.Y. Lee, Lab scale experiments for permeable reactive barriers against contaminated groundwater with ammonium and heavy metals using clinoptilolite (01-29B), J. Hazard. Mater. 95 (2002) 65–79.
[8] B. Yuncu, D.F. Sanin, U. Yetis, An investigation of heavy metal biosorption in relation to C/N ratio of activated sludge, J. Hazard. Mater. 137 (2006) 990–997.
[9] G. Bartzas, K. Komnitsas, Solid phase studies and geochemical modelling of low-cost permeable reactive barriers, J. Hazard. Mater. 183 (2010) 301–308.
[10] T. Suponik, Adsorption and biodegradation in PRB technology, Environ. Protection Eng. 36 (2010) 43–57.
[11] A.A.H. Faisal, Z.A. Hmood, Groundwater protection from cadmium contamination by zeolite permeable reactive barrier, Desalin. Water Treat. (2013) doi:10.1080/19443994.2013.855668.
[12] G.S.D. Ambrosini, Reactive Materials for Subsurface Remediation Through Permeable Reactive Barriers, Ph.D Thesis, Swiss Federal Institute of Technology, Zurich, 2004.
[13] A.Z. Woinarski, G.W. Stevens, I. Snape, A natural zeolite permeable reactive barrier to treat heavy-metal contaminated waters in Antarctica, Process Saf. Environ. Prot. 84(2) (2006) 109–116.
[14] L. Geranio, Review of Zero Valent Iron and Apatite as Reactive Materials for Permeable Reactive Barrier, Term Paper SS 07/08, Major in Biogeochemistry and Pollutant Dynamics, Department of Environmental Science ETH Zurich, 2007.

[15] G. Bazdanis, K. Komnitsas, E. Sahinkaya, D. Zaharaki, Removal of heavy metals from leachates using permeable reactive barriers filled with reactive organic/inorganic mixtures, Proceedings of the 3rd International Conference on Environmental Management, Engineering, Planning, and Economics (CEMEPE) & SECOTOX Conference, June 19–24, 2011, Skiathos island, Greece.
[16] C.O. Plamondon, R. Lynch, A. Al-Tabbaa, Metal retention experiments for the design of soil-mix technology permeable reactive barriers, Clean—Soil, Air, Water 39 (2011) 844–852.
[17] T. Suponik, Groundwater treatment with the use of zero-valent iron in the permeable reactive barrier technology, Physicochem. Prob. Miner. Process 49 (2013) 13–23.
[18] A. Mathews, I. Zayas, Particle size and shape effects on adsorption rate parameters, J. Environ. Eng. 115 (1989) 41–55.
[19] S. Wang, Z. Nan, Y. Li, Z. Zhao, The chemical bonding of copper ions on kaolin from Suzhou, China, Desalination 249 (2009) 991–995.
[20] O. Hamdaoui, E. Naffrechoux, Modeling of adsorption isotherms of phenol and chlorophenols onto granular activated carbon part I. Two-parameter models and equations allowing determination of thermodynamic parameters, J. Hazard. Mater. 147 (2007) 381–394.
[21] J.P. Chen, L. Wang, S.W. Zou, Determination of lead bio-sorption properties by experimental and modeling simulation study, Chem. Eng. J. 131 (2008) 209–215.
[22] K.M. Doke, M. Yusufi, R.D. Joseph, E.M. Khan, Biosorption of hexavalent chromium onto wood apple shell: Equilibrium, kinetic and thermodynamic studies, Desalin. Water Treat. 50 (2012) 170–179.
[23] M. Alkan, B. Kalay, M. Doğan, Ő. Demirbaş, Removal of copper ions from aqueous solutions by kaolinite and batch design, J. Hazard. Mater. 153 (2008) 867–876.
[24] M. Selvarani, P. Prema, Removal of toxic metal hexavalent chromium [Cr(VI)] from aqueous solution using starch—Stabilized nanoscale zero valent iron as adsorbent: Equilibrium and kinetics, Int. J. Environ. Sci. 2 (2010) 1962–1975.
[25] M.P. Anderson, W.W. Woessner, Applied Groundwater Modeling: Simulation of Flow and Advective Transport, second ed., Academic Press, San Diego, CA, 1992.